

# Generation of entanglement for two trapped ions in thermal motion with an extended Jonathan–Plenio–Knight method

Hiroo Azuma<sup>\*</sup>

Global Research Center for Quantum Information Science,  
National Institute of Informatics,  
2-1-2 Hitotsubashi, Chiyoda-ku, Tokyo 101-8430, Japan

December 16, 2021

## Abstract

We investigate an extension of Jonathan, Plenio, and Knight’s light-shift-induced quantum gate for a trapped ion quantum computer. In our method, we generate entanglement between two ions by illuminating each of them simultaneously with its own allocated laser field, where these laser fields are equal in frequency but have a phase difference of  $\pi$ . In this process, we adjust an operation time to obtain the maximally entangled state of the two cold ions, that is to say, the number of centre-of-mass mode phonons is equal to zero. However, our scheme cannot generate the maximally entangled state if the phonons exist because of thermal fluctuation. To overcome this problem, we examine how to gain the Bell state with high fidelity for the case where a single phonon exists with applying the optimized unitary transformation to the ion and the phonon mode. In our concrete example, this optimum correction allows us to acquire the Bell state with fidelity 0.95 on condition that the mean phonon number in thermal equilibrium is equal to 0.200 at most. The switching rate of our proposal is higher than that of Cirac and Zoller’s quantum gate.

## 1 Introduction

Since Preskill put forward a concept of noisy intermediate-scale quantum (NISQ) technology, many researchers have devoted themselves to the development of quantum computers composed of about 50 to 100 qubits [1]. The most well-known work that heralded the beginning of the NISQ era was the demonstration of quantum supremacy by Arute *et al.*

---

<sup>\*</sup>hiroo.azuma@m3.dion.ne.jp, zuma@nii.ac.jp. On leave from Nisshin-scientia Co., Ltd., 8F Omori Belport B, 6-26-2 MinamiOhi, Shinagawa-ku, Tokyo 140-0013, Japan.

using a 53-qubit quantum computer [2]. In Ref. [2], Arute *et al.* performed a task of sampling the output of a pseudo-random circuit with the programmable quantum computer made up of 53 functional qubits and obtained a million samples within 200 seconds. They asserted that it took 10 000 years to finish this task with the most modern supercomputer. Their quantum processor was comprised of a two-dimensional array of transmon qubits. The transmon is a kind of superconducting charge qubit and it was proposed theoretically for the first time by Koch *et al.* in 2007 [3]. It is regarded as being sturdy to withstand a charge noise.

Although superconducting quantum computing attracts the attention of researchers and the result of Arute *et al.* is considered to be a notable milestone, there are alternative methods for constructing quantum processors [4, 5, 6]. The most typical approach of these alternatives is the ion trap quantum computing. In Ref. [7], the practical realization of a fully controlled 20-qubit processor was reported, and we can recognize it as the NISQ computer.

The first theoretical proposal of the trapped ion quantum computation was provided by Cirac and Zoller in 1995 [8]. Since this proposition, aggressive research activities have been conducted and experimental technologies for the actual implementation of ion trap quantum computing were extremely refined in recent years. For example, implementation of a full quantum algorithm was accomplished with the trapped ion system in 2003 [9]. In this experiment, two  $^{40}\text{Ca}^+$  ions are used for carrying out the Deutsch–Jozsa algorithm.

How to scale up a small quantum register composed of trapped ions to large numbers of qubits was discussed in Ref. [10]. In Ref. [10], the quantum charge-coupled device architecture was proposed. In this architecture, the ions are stored in the memory region and moved to the interaction region for logic operations. Both regions are implemented as traps and the ions are manipulated by changing the voltage of these traps.

The trapped ion quantum computer has the following salient features. Reference [11] reported that a coherence time of over ten minutes was observed for a single qubit in a trapped ion system. In Ref. [12], a qubit was constructed from a single trapped calcium ion and its readout fidelity attained 99.77%. In Ref. [13], by using the hyperfine states in the ground  $4\text{S}_{1/2}$  levels of the  $^{43}\text{Ca}^+$  ion, qubit state preparation and single-shot readout fidelity reached 99.93%. Reference [13] also showed a single-qubit gate fidelity of 99.9999%. The ion trap quantum computation is suitable for generating entanglement between two qubits, as well. Experimentally, an error rate for generation of the Bell state was estimated at  $8 \times 10^{-4}$  in Ref. [14], and fidelity of the two-qubit gate attained 99.9% in Ref. [15]. In Ref. [16], a protocol for simultaneously entangling arbitrary pairs of qubits on an ion-trap quantum computer was proposed theoretically. Thus, this protocol realizes multiple two-qubit gates.

Although Cirac and Zoller's original proposal is excellent, it has the following two disadvantages. The first one is a low switching rate of the ion–phonon gate that generates entanglement. (The phonon is the centre-of-mass vibrational mode of the ion chain.) The second one is vulnerability to thermal noise caused by fluctuations of phonons at finite temperature. Comprehensive reviews of ion trap quantum computing were provided in Refs. [17, 18, 19, 20].

An attempt to resolve the first problem theoretically was made in Ref. [21] by Jonathan, Plenio, and Knight. In Ref. [21], using the ac Stark shift induced by light

being resonant with the ionic transition frequency, a fast ion–phonon gate generating entanglement was implemented. In this method, they adjusted the Rabi frequency of laser light applied to the ion to a specific value and cause the Jaynes–Cummings interaction between the ion and the phonon. They constructed a two-qubit gate from a combination of ion–phonon gates and one-qubit rotation gates. This process is faster than Cirac and Zoller’s method. However, this scheme is sensitive to the thermal motion of phonons. It suffers from thermal noise if the number state of phonons is not given by  $|0\rangle_P$  but they obey the Bose–Einstein statistics at finite temperature.

An attempt to resolve the second problem was made in Refs. [22, 23] by Mølmer and Sørensen. The implementation of their gate was illuminating two ions with a bichromatic laser light simultaneously. In this scenario, if we calculate a perturbation theory of interaction among two ions and the phonon mode, the first-order energy shift disappears and the second-order correction becomes essential. When we sum all second-order terms to which intermediate states contribute, miracle interference occurs and the total energy shift does not rely on the number of the phonons at all. This fact indicates that the generation of the quantum entanglement between the two ions with Mølmer–Sørensen gate is nothing to do with the freedom of the phonon mode. Thus, even if the phonons obey the thermal distribution, the Mølmer–Sørensen gate between the two ions does not suffer from thermal noise at all.

The only drawback of the Mølmer–Sørensen gate is a low switching rate, that is to say, it works much more slowly than the Cirac and Zoller’s ion–phonon gate. This is because the second-order correction of the effective Hamiltonian of the Mølmer–Sørensen gate is in proportion to  $(\eta\Omega)^2/(\omega_z - \delta)$ , where  $\Omega$  and  $\omega_0 \pm \delta$  represent the Rabi frequency and net angular frequencies of the bichromatic laser light, respectively,  $\hbar\omega_0$  denotes the energy difference between two levels of the ion, and  $\omega_z$  represents the angular frequency of the phonon. We assume  $\Omega \ll \omega_z$  and set  $\delta$  to a value being close to but not resonant with  $\omega_z$ . Moreover, we assume  $\eta \ll 1$ , where  $\eta$  denotes the Lamb–Dicke parameter. (In actual numerical calculations of Ref. [23], the authors assumed  $\Omega = 0.10\omega_z$ ,  $\delta = 0.90\omega_z$ , and  $\eta = 0.10$ .) Thus, the frequency of the Mølmer–Sørensen gate determined by the second-order perturbation theory becomes quite small and it makes the operation time very long.

In this paper, we try combining these two ideas, the Jonathan–Plenio–Knight gate and the Mølmer–Sørensen gate. In concrete terms, we illuminate each of two ions simultaneously with its own allocated laser field, where these laser fields are equal in frequency but have a phase difference  $\pi$ . We set the net frequency and the Rabi frequency of these laser fields to the ionic transition frequency and half the phonon frequency, respectively. Applying these laser fields to two ions, we can transform a separable state of the two cold ions into the maximally entangled state.

However, our scheme does not witness a miracle cancellation of the freedom of the phonon mode as shown in the Mølmer–Sørensen gate, so that it is sensitive to the thermal noise caused by the phonon mode. To overcome this trouble, we apply the optimized unitary transformation to the ion and the phonon mode with thermal fluctuation. This optimum unitary transformation allows us to acquire the maximally entangled state with relatively high fidelity in the case where the number of phonons is equal to one. From this method, in a concrete example examined in the latter part of our study, we show that we

can generate the maximally entangled state with the fidelity of 0.95 under the condition that the average number of thermal phonons is given by  $n_{\text{th}} \leq 0.200$ .

Important points of the dynamics of our scheme is as follows. Describing the two-level state of the ion as  $\{|g\rangle, |e\rangle\}$  and letting the initial state of ions A, B, and the phonon be given by  $|\psi(0)\rangle = |g\rangle_A|g\rangle_B|0\rangle_P$ , we obtain probabilities,  $|_A\langle g|_B\langle g|_P\langle 0|\psi(t)\rangle|^2$  and  $|_A\langle e|_B\langle e|_P\langle 0|\psi(t)\rangle|^2$ , as functions of time  $t$ . Then, curves of these probabilities exhibit interference patterns of beats. The high and low frequencies of these beats are given by  $\eta^2\omega_z$  and  $\eta\omega_z$ , respectively. (Thus, the frequency of the envelopes of the beats is equal to  $\eta^2\omega_z$ .) Corresponding periods are given by  $T_1 \sim (\eta^2\omega_z)^{-1}$  and  $T_2 \sim (\eta\omega_z)^{-1}$ , respectively. When amplitudes of these envelopes for  $|_A\langle g|_B\langle g|_P\langle 0|\psi(t)\rangle|^2$  and  $|_A\langle e|_B\langle e|_P\langle 0|\psi(t)\rangle|^2$  are equal to 1/2 with each other, we can expect that the state of the two ions is maximally entangled. Thus, we can roughly estimate the operation time of our quantum gate at  $T_1/4$ .

The time required for the creation of the Bell state from a separable state with our scheme is longer than that with the Jonathan–Plenio–Knight gate, but shorter than that with the Cirac–Zoller gate. We need to let the phase difference of two laser fields applied to two ions be equal to  $\pi$  for our scheme. If the two laser fields do not have a nonzero phase difference, the beats do not appear.

This paper is organized as follows. In Sec. 2, we review bases of ion trap quantum computing and Jonathan, Plenio, and Knight’s light-shift-induced quantum gate. In Sec. 3, we consider the extension of the Jonathan–Plenio–Knight gate. In Sec. 4, preparing the initial state  $|g\rangle_A|g\rangle_B|0\rangle_P$ , we investigate the time evolution of our process. In Sec. 5, preparing the initial state  $|g\rangle_A|g\rangle_B|1\rangle_P$ , we examine the time evolution of our process. In Sec. 6, we investigate how to remove effects of thermal noise caused by fluctuation of the phonon mode governed by the Bose–Einstein statics at finite low temperature. In Sec. 7, we compare the operation times of Cirac–Zoller gate, Jonathan–Plenio–Knight gate, and our process. In Sec. 8, we carry out numerical simulations of our process affected by the thermal noise of the phonon mode. In Sec. 9, we provide discussions.

## 2 Reviews of bases of ion trap quantum computing and Jonathan, Plenio, and Knight’s light-shift-induced quantum gate

First, we explain the Hamiltonian of the ion trap quantum computer. This part is a review of Refs. [8, 17, 18, 19, 20].

Due to a linear Paul-rf trap, ions are confined by a static harmonic potential well in two dimensions ( $x$  and  $y$ ) along the  $z$ -axis. The ions in the potential repel each other via the repulsive Coulomb force and are trapped in a string-like configuration. The ions are placed at equal intervals like a one-dimensional chain of masses connected to springs. This string of ions creates phonons as quantized modes of vibrations.

We assume that each ion has a magnetic dipole moment  $\boldsymbol{\mu}_m$  and interacts with a magnetic flux density  $\mathbf{B}$ . Then, its Hamiltonian is given by  $H_I = -\boldsymbol{\mu}_m \cdot \mathbf{B}$ . Because the magnetic dipole moment is proportional to the spin operator, we regard spin ‘down’ and

‘up’ as states of the qubit  $|0\rangle$  and  $|1\rangle$ , respectively.

To perform quantum logic gates, we apply laser fields to the ions. Here, we consider  $\mathbf{B}$  to be a uniform wave propagating along the  $z$  direction and being polarized in the  $x$  direction,

$$\mathbf{B} = B\hat{\mathbf{x}} \cos(kz - \omega t + \phi), \quad (1)$$

where  $\hat{\mathbf{x}}$  denotes a unit vector in the direction of  $x$ . Then, we can express the Hamiltonian  $H_I$  as

$$H_I = 2\hbar\Omega\sigma_x[e^{i(kz-\omega t+\phi)} + e^{-i(kz-\omega t+\phi)}], \quad (2)$$

where  $\mu_m = -(\mu_m/2)(\sigma_x, \sigma_y, \sigma_z)$  and  $\Omega = -\mu_m B/(8\hbar)$ .

Next, we quantize the centre-of-mass mode of the phonons by rewriting the coordinate variable  $z$  with annihilation and creation operators  $a^\dagger$  and  $a$  in the form

$$z = z_0(a + a^\dagger). \quad (3)$$

Thus, the interaction Hamiltonian  $H_I$  is given by

$$H_I = \hbar\Omega(\sigma_+ + \sigma_-)\{\exp[i\eta(a + a^\dagger) - i\omega t + i\phi] + \exp[-i\eta(a + a^\dagger) + i\omega t - i\phi]\}, \quad (4)$$

where  $\sigma_\pm = \sigma_x \pm i\sigma_y$  and  $\eta = kz_0$ . We assume that the Lamb–Dicke parameter  $\eta$  is very small, *i.e.*,  $\eta \ll 1$ . The meaning of this inequality is as follows. The Lamb–Dicke parameter  $\eta$  is a product of  $z_0$ , the width of the potential well along the direction of  $z$  in which all the ions are confined, and  $k$ , the wavenumber of incident laser light. Letting  $\lambda$  represent the wavelength of the laser light, we obtain  $k = 2\pi/\lambda$ . To make the confined ion not jump out of the potential well, we must make an assumption  $\lambda \gg z_0$ . This assumption provides the Lamb–Dicke parameter’s condition  $\eta \ll 1$ .

The Hamiltonian of the ion and the centre-of-mass mode without their interaction is given by

$$H_0 = \frac{1}{2}\hbar\omega_0\sigma_z + \hbar\omega_z a^\dagger a. \quad (5)$$

From now on, we describe the system with the interaction picture. Thus, we define the following unitary transformation:

$$U_0 = \exp[i(H_0/\hbar)t]. \quad (6)$$

Then, we obtain a new Hamiltonian in the form

$$\begin{aligned} H'_I &= U_0 H_I U_0^\dagger \\ &= \hbar\Omega[\sigma_+ \exp(i\omega_0 t) + \sigma_- \exp(-i\omega_0 t)] \\ &\quad \times \left( \exp\{i\eta[a \exp(-i\omega_z t) + a^\dagger \exp(i\omega_z t)] - i\omega t + i\phi\} \right. \\ &\quad \left. + \exp\{-i\eta[a \exp(-i\omega_z t) + a^\dagger \exp(i\omega_z t)] + i\omega t - i\phi\} \right). \end{aligned} \quad (7)$$

Here, we eliminate terms  $\exp[\pm i(\omega + \omega_0)t]$  in Eq. (7) according to the rotating wave approximation. This approximation corresponds to an assumption of  $(\omega + \omega_0)T \gg 1$

where  $T$  is a typical operation time for the quantum gate realized by this Hamiltonian. Thus, we obtain an approximate Hamiltonian

$$H'_I \simeq \hbar\Omega\sigma_+ \exp\{i\eta[a \exp(-i\omega_z t) + a^\dagger \exp(i\omega_z t)] - i\delta t + i\phi\} + \hbar\Omega\sigma_- \exp\{-i\eta[a \exp(-i\omega_z t) + a^\dagger \exp(i\omega_z t)] + i\delta t - i\phi\}, \quad (8)$$

where  $\delta = \omega - \omega_0$ . For the sake of simplicity, we suppose  $\phi = 0$ . Equation (8) is a basic Hamiltonian of the ion trap quantum computing.

Second, we explain Jonathan, Plenio, and Knight's light-shift-induced quantum gate. This part is a review of Ref. [21].

First of all, we assume  $\delta = 0$ , that is to say, we apply laser light with the angular frequency  $\omega = \omega_0$  to the ion. Then, the condition of the rotating wave approximation changes into  $2\omega_0 T \gg 1$ . Moreover, in order to leave terms  $\exp(\pm i\omega_z t)$  in  $H'_I$ , we must suppose  $\omega_0 \gg \omega_z$ .

Because of the condition of the Lamb–Dicke parameter  $\eta \ll 1$ , we derive approximate  $H'_I$  up to the second-order terms for  $\eta$  in the form

$$H'_I = \hbar\Omega\{\sigma_+ + \sigma_- + i\eta(\sigma_+ - \sigma_-)[a \exp(-i\omega_z t) + a^\dagger \exp(i\omega_z t)] - \frac{1}{2}\eta^2(\sigma_+ + \sigma_-)[a \exp(-i\omega_z t) + a^\dagger \exp(i\omega_z t)]^2\} + O(\eta^3). \quad (9)$$

Until now, we consider eigenvectors of the operator  $\sigma_z$ ,  $\{|0\rangle, |1\rangle\}$ , as the two-level states of the ion. From now on, we regard  $|\pm\rangle = (1/\sqrt{2})(|0\rangle \pm |1\rangle)$  as the computational basis states rather than  $\{|0\rangle, |1\rangle\}$ . In concrete terms, relationships between these basis vectors are given by

$$|g\rangle = |0\rangle = \begin{pmatrix} 0 \\ 1 \end{pmatrix}, \quad |e\rangle = |1\rangle = \begin{pmatrix} 1 \\ 0 \end{pmatrix}, \quad (10)$$

$$\tilde{R} = R_y(-\frac{\pi}{2}) = \frac{1}{\sqrt{2}} \begin{pmatrix} 1 & 1 \\ -1 & 1 \end{pmatrix}, \quad (11)$$

$$|+\rangle = \tilde{R}|0\rangle, \quad |-\rangle = \tilde{R}|1\rangle. \quad (12)$$

These relationships imply that we must change the Hamiltonian into a new one as  $H'_I \rightarrow \tilde{R}H'_I\tilde{R}^\dagger$ .

Using a formula

$$\tilde{R}\sigma_\pm\tilde{R}^\dagger = \frac{1}{2}[\sigma_z \pm (\sigma_+ - \sigma_-)], \quad (13)$$

we can rewrite the Hamiltonian given by Eq. (9) as

$$\tilde{R}H'_I\tilde{R}^\dagger = H''_0 + H''_I, \quad (14)$$

$$H''_0 = \hbar\Omega\sigma_z, \quad (15)$$

$$H''_I = \hbar\Omega\{\eta(\sigma_+ - \sigma_-)[a \exp(-i\omega_z t) + a^\dagger \exp(i\omega_z t)] - \frac{1}{2}\eta^2\sigma_z[a \exp(-i\omega_z t) + a^\dagger \exp(i\omega_z t)]^2\} + O(\eta^3). \quad (16)$$

Here, we make a further ‘interaction picture’ transformation with the Hamiltonian  $H_0''$  that does not contain interaction terms. Defining a unitary transformation

$$U_0'' = \exp[i(H_0''/\hbar)t], \quad (17)$$

we obtain

$$\begin{aligned} U_0'' H_I'' U_0''^\dagger &= i\eta\hbar\Omega\{\exp[i(2\Omega - \omega_z)t]\sigma_+a - \exp[-i(2\Omega - \omega_z)t]\sigma_-a^\dagger \\ &\quad + \exp[i(2\Omega + \omega_z)t]\sigma_+a^\dagger - \exp[-i(2\Omega + \omega_z)t]\sigma_-a\} \\ &\quad - \frac{1}{2}\eta^2\hbar\Omega\sigma_z[a\exp(-i\omega_zt) + a^\dagger\exp(i\omega_zt)]^2 + O(\eta^3). \end{aligned} \quad (18)$$

Now, setting  $\Omega = \omega_z/2$ , we obtain an approximate Hamiltonian of Eq. (18) in the form

$$H_I \simeq \frac{i}{2}\eta\hbar\omega_z(\sigma_+a - \sigma_-a^\dagger) - \frac{1}{4}\eta^2\hbar\omega_z\sigma_z(a^\dagger a + a a^\dagger), \quad (19)$$

where we neglect the terms  $\exp(\pm 2i\omega_z t)$  in Eq. (18) because of the rotating wave approximation. This treatment requires a condition  $T\omega_z \gg 1$ , where  $T$  represents a typical operation time of this gate. All the conditions of the rotating wave approximation are gathered together into the following inequality:

$$T\omega_0 \gg T\omega_z \gg 1. \quad (20)$$

Contrastingly, if we set  $\Omega = -\omega_z/2$ , the Hamiltonian of Eq. (18) is estimated at

$$H_I \simeq -\frac{i}{2}\eta\hbar\omega_z(\sigma_+a^\dagger - \sigma_-a) + \frac{1}{4}\eta^2\hbar\omega_z\sigma_z(a^\dagger a + a a^\dagger), \quad (21)$$

where we remove terms  $\exp(\pm 2i\omega_z t)$  due to the rotating wave approximation. These Hamiltonians given by Eqs. (19) and (21) realize the Jonathan–Plenio–Knight gate.

### 3 An extension of the Jonathan–Plenio–Knight gate

We present our novel results in this section.

We apply operations of the Jonathan–Plenio–Knight gate to two ions A and B. We illuminate ions A and B with laser light of  $\omega = \omega_0$  and  $\Omega = \omega_z/2$  and that of  $\omega = \omega_0$  and  $\Omega = -\omega_z/2$ , respectively. Because these laser fields fed into ions A and B have a phase difference  $\pi$ , we draw attention to the fact that their amplitudes have opposite signs. Thus, from Eqs. (19) and (21), the total Hamiltonian is given by

$$\begin{aligned} H &= \frac{i}{2}\eta\hbar\omega_z(\sigma_{A+}a - \sigma_{A-}a^\dagger) - \frac{i}{2}\eta\hbar\omega_z(\sigma_{B+}a^\dagger - \sigma_{B-}a) \\ &\quad - \frac{1}{4}\eta^2\hbar\omega_z(\sigma_{Az} - \sigma_{Bz})(a a^\dagger + a^\dagger a). \end{aligned} \quad (22)$$

Here, to examine the time evolution of a state of the ions A, B, and the phonons caused by this Hamiltonian, we give its explicit expression. From now on, we describe

the basis vectors of the ion A,  $|0\rangle_A$  and  $|1\rangle_A$ , as  $|g\rangle_A$  and  $|e\rangle_A$ , respectively, for the sake of clarity. For the basis vectors of the ion B, we use the same notation. Moreover, we write the number states of the phonons as  $|n\rangle_P$  for  $n = 0, 1, 2, \dots$

First, we examine the case where the initial state is given by  $|g, g, 0\rangle = |g\rangle_A|g\rangle_B|0\rangle_P$ . In this case, we only need to consider three orthonormal vectors  $\{|g, g, 0\rangle, |e, e, 0\rangle, |g, e, 1\rangle\}$ . Because of

$$aa^\dagger + a^\dagger a = 1 + 2a^\dagger a, \quad (23)$$

we can describe matrix elements of the Hamiltonian as

$$H = \frac{1}{2}\eta\hbar\omega_z \begin{pmatrix} 0 & 0 & i \\ 0 & 0 & i \\ -i & -i & 3\eta \end{pmatrix}, \quad (24)$$

where the basis vectors are given by  $\{|g, g, 0\rangle, |e, e, 0\rangle, |g, e, 1\rangle\}$ .

Next, we consider the case where the initial state is given by  $|g, g, n\rangle$  for  $n \geq 1$ . In this case, we only need to examine four orthonormal vectors  $\{|g, g, n\rangle, |e, e, n\rangle, |g, e, n+1\rangle, |e, g, n-1\rangle\}$ . Matrix elements of the Hamiltonian with these four basis vectors are given by

$$H = \frac{1}{2}\eta\hbar\omega_z \begin{pmatrix} 0 & 0 & i\sqrt{n+1} & -i\sqrt{n} \\ 0 & 0 & i\sqrt{n+1} & -i\sqrt{n} \\ -i\sqrt{n+1} & -i\sqrt{n+1} & (2n+3)\eta & 0 \\ i\sqrt{n} & i\sqrt{n} & 0 & -(2n-1)\eta \end{pmatrix}. \quad (25)$$

## 4 The case where the initial state is prepared as $|g, g, 0\rangle$

We examine the time evolution of the state that is initially prepared as  $|g, g, 0\rangle$ . In this case, the Hamiltonian is described in Eq. (24), and we obtain its eigenvalues and eigenvectors as

$$\begin{aligned} \lambda_1 &= 0, \\ \lambda_2 &= \frac{1}{4}\eta[3\eta - x(\eta)]\hbar\omega_z, \\ \lambda_3 &= \frac{1}{4}\eta[3\eta + x(\eta)]\hbar\omega_z, \end{aligned} \quad (26)$$

$$\begin{aligned} \mathbf{v}_1 &= \frac{1}{\sqrt{2}}(-1, 1, 0)^T, \\ \mathbf{v}_2 &= -\frac{i}{2}\sqrt{1 + \frac{3\eta}{x(\eta)}}(1, 1, \frac{4i}{\sqrt{8 + 6\eta[3\eta + x(\eta)]}})^T, \\ \mathbf{v}_3 &= \frac{i}{2}\sqrt{1 - \frac{3\eta}{x(\eta)}}(1, 1, -\frac{i}{2}[3\eta + x(\eta)])^T, \end{aligned} \quad (27)$$

where

$$x(\eta) = \sqrt{8 + 9\eta^2}. \quad (28)$$

Here, we define the following unitary transformation

$$V = \begin{pmatrix} \mathbf{v}_1^\dagger \\ \mathbf{v}_2^\dagger \\ \mathbf{v}_3^\dagger \end{pmatrix}. \quad (29)$$

Then, the unitary operator for the time evolution is given by

$$U = V^\dagger \begin{pmatrix} \exp(-i\lambda_1 t) & 0 & 0 \\ 0 & \exp(-i\lambda_2 t) & 0 \\ 0 & 0 & \exp(-i\lambda_3 t) \end{pmatrix} V. \quad (30)$$

Setting the initial state to  $|\psi(t=0)\rangle = |g, g, 0\rangle = (1, 0, 0)^T$ , we obtain the state at arbitrary time  $t$  in the form

$$\begin{aligned} |\psi(t)\rangle &= U|\psi(0)\rangle \\ &= c_1(t)|g, g, 0\rangle + c_2(t)|e, e, 0\rangle + c_3(t)|g, e, 1\rangle, \end{aligned} \quad (31)$$

$$\begin{aligned} c_1(t) &= \frac{1}{2} + \frac{1}{4} \exp\left[-\frac{i}{4}\eta r(\eta)\omega_z t\right] \{q(\eta) + s(\eta) \exp\left[\frac{i}{2}\eta x(\eta)\omega_z t\right]\}, \\ c_2(t) &= -1 + c_1(t), \\ c_3(t) &= \frac{i}{x(\eta)} \exp\left[-\frac{i}{4}\eta r(\eta)\omega_z t\right] \{-1 + \exp\left[\frac{i}{2}\eta x(\eta)\omega_z t\right]\}, \end{aligned} \quad (32)$$

where

$$\begin{aligned} r(\eta) &= 3\eta + x(\eta), \\ s(\eta) &= 1 + \frac{3\eta}{x(\eta)}, \\ q(\eta) &= 1 - \frac{3\eta}{x(\eta)}. \end{aligned} \quad (33)$$

Because of  $\eta \ll 1$ , we obtain the first-order approximation of  $x(\eta)$ ,  $r(\eta)$ ,  $s(\eta)$ , and  $q(\eta)$  as

$$\begin{aligned} x(\eta) &\simeq 2\sqrt{2}, \\ r(\eta) &\simeq 3\eta + 2\sqrt{2}, \\ s(\eta) &\simeq 1 + \frac{3\eta}{2\sqrt{2}}, \\ q(\eta) &\simeq 1 - \frac{3\eta}{2\sqrt{2}}, \end{aligned} \quad (34)$$

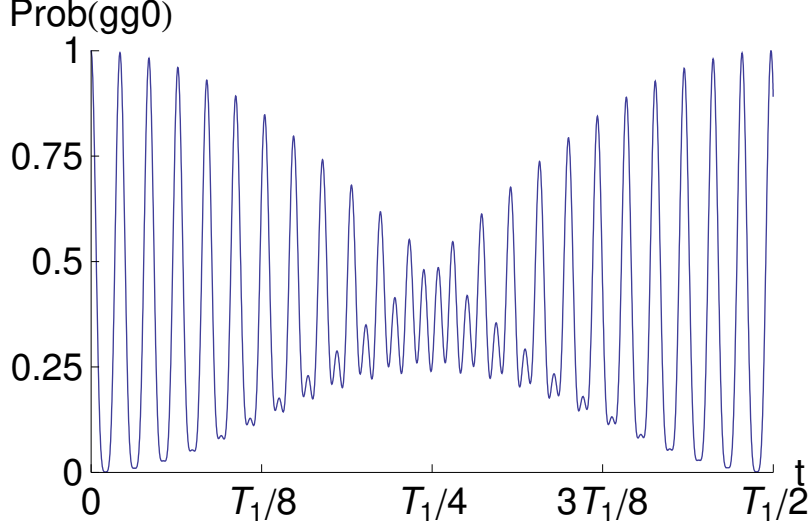


Figure 1: A graph of  $|c_1(t)|^2$ , the probability that we observe  $|g, g, 0\rangle$ , as a function of time  $t$  derived from Eq. (32) with  $\omega_z = 10$  and  $\eta = 0.02$ . A curve of the graph forms the beat whose long and short periods are given by  $T_1$  and  $T_2^{(0)}$ , respectively. The amplitude of the envelope with the period  $T_1$  is nearly equal to  $1/2$  around  $t = T_1/4$ .

and we rewrite the coefficients  $c_1(t)$ ,  $c_2(t)$ , and  $c_3(t)$  in the form

$$\begin{aligned}
 c_1(t) &\simeq \frac{1}{2} + \frac{1}{8} \exp(-i\frac{3}{4}\eta^2\omega_z t) [4 \cos(\frac{\eta\omega_z t}{\sqrt{2}}) + i3\sqrt{2}\eta \sin(\frac{\eta\omega_z t}{\sqrt{2}})], \\
 c_2(t) &\simeq -1 + c_1(t), \\
 c_3(t) &\simeq \frac{i}{2\sqrt{2}} \exp[-\frac{i}{4}\eta(2\sqrt{2} + 3\eta)\omega_z t] [-1 + \exp(i\sqrt{2}\eta\omega_z t)] \\
 &\simeq -\frac{1}{\sqrt{2}} \sin(\frac{\eta\omega_z t}{\sqrt{2}}).
 \end{aligned} \tag{35}$$

In the above equation of  $c_3(t)$ , we replace  $\exp[-(i/4)\eta(2\sqrt{2} + 3\eta)\omega_z t]$  with  $\exp[-(i/\sqrt{2})\eta\omega_z t]$  for the approximation.

From Eq. (35), we notice the following facts. The curves of  $c_1(t)$  and  $c_2(t)$  as functions of time  $t$  form beats whose long and short periods are given by  $T_1$  and  $T_2^{(0)}$ , respectively, where

$$T_1 = \frac{8\pi}{3\eta^2\omega_z}, \tag{36}$$

$$T_2^{(0)} = \frac{2\sqrt{2}\pi}{\eta\omega_z}. \tag{37}$$

Thus, the angular frequency and period of the envelope of the beats are equal to  $\eta^2\omega_z$  and  $T_1$ , respectively. The curve of  $c_3(t)$  is described by a sine wave with an amplitude  $1/\sqrt{2}$  and a period  $T_2^{(0)}$ .

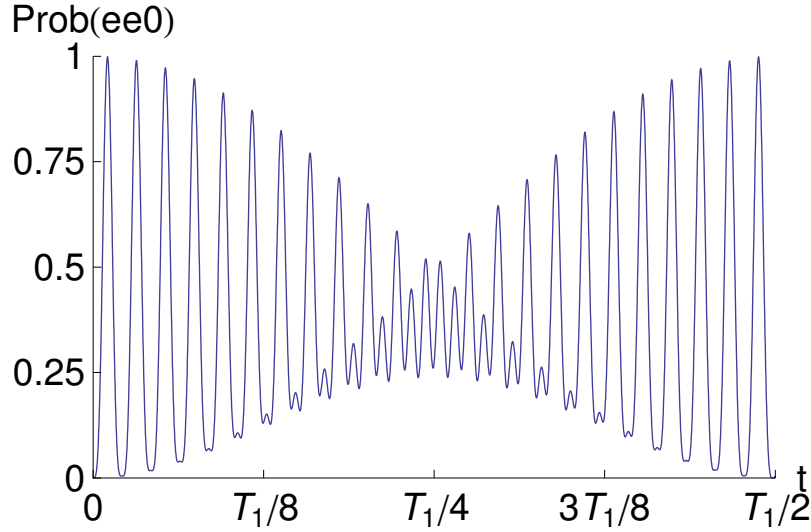


Figure 2: A graph of  $|c_2(t)|^2$ , the probability that we observe  $|e, e, 0\rangle$ , as a function of time  $t$  derived from Eq. (32) with  $\omega_z = 10$  and  $\eta = 0.02$ . A curve of the graph forms the beat whose long and short periods are given by  $T_1$  and  $T_2^{(0)}$ , respectively. The amplitude of the envelope with the period  $T_1$  is nearly equal to  $1/2$  around  $t = T_1/4$ .

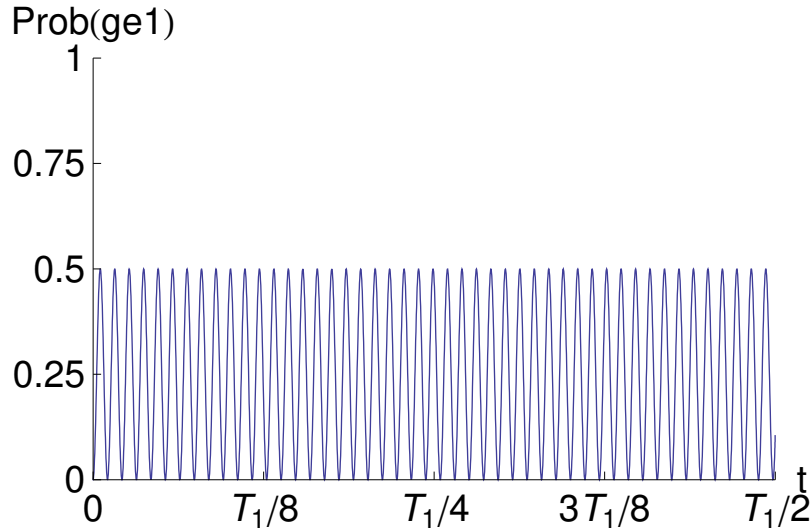


Figure 3: A graph of  $|c_3(t)|^2$ , the probability that we observe  $|g, e, 1\rangle$ , as a function of time  $t$  derived from Eq. (32) with  $\omega_z = 10$  and  $\eta = 0.02$ . A curve of the graph is given by a square of a sine wave whose amplitude and period are equal to  $1/2$  and  $T_2^{(0)}$ , respectively.

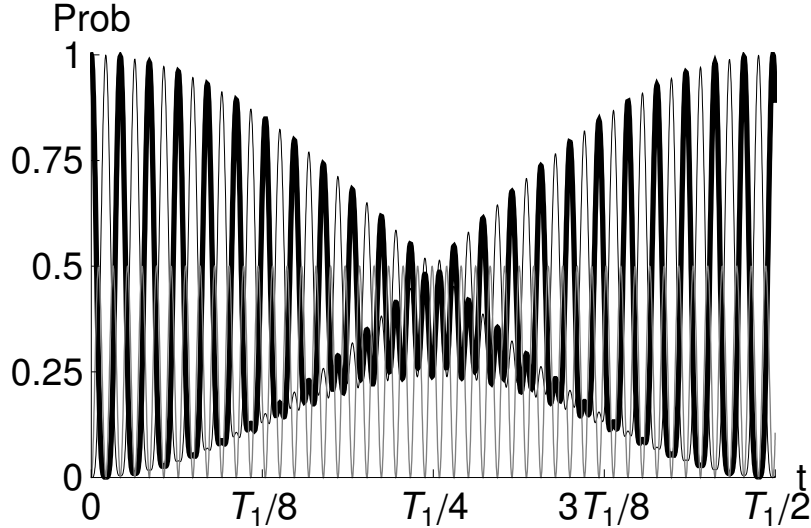


Figure 4: Figures 1, 2, and 3 are overlaid with each other. The black thick, black thin, and grey curves represent  $|c_1(t)|^2$ ,  $|c_2(t)|^2$ , and  $|c_3(t)|^2$ , respectively. We can expect that  $|c_1(t)|^2 \simeq |c_2(t)|^2 \simeq 1/2$  and  $|c_3(t)|^2 \simeq 0$  hold near the time  $t = T_1/4$ .

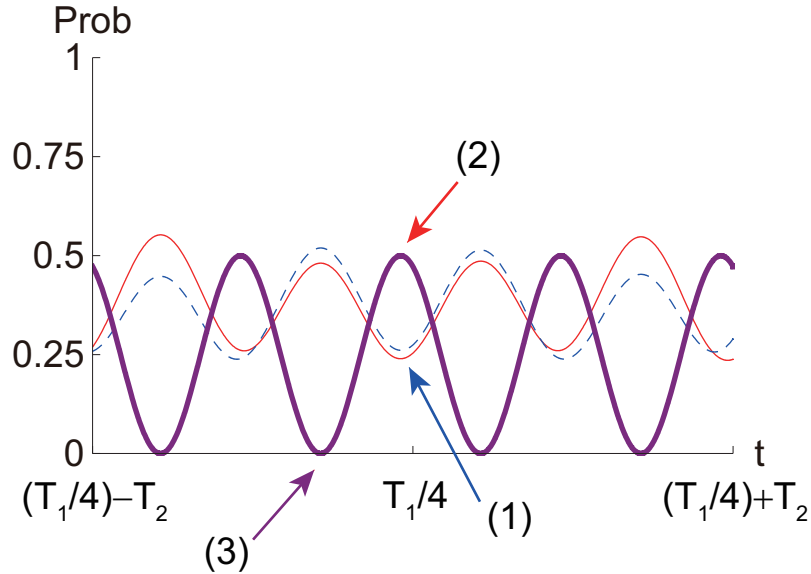


Figure 5: An enlarged view of Fig. 4 in the range of  $(T_1/4) - T_2 \leq t \leq (T_1/4) + T_2$ . The red curve, the blue dashed curve, and purple thick curve represent  $|c_1(t)|^2$ ,  $|c_2(t)|^2$ , and  $|c_3(t)|^2$ , respectively. Around  $t \simeq 522$  that is somewhat earlier than  $t = T_1/4$ , a blue arrow (1) and a red arrow (2) indicate the local minimums of  $|c_1(t)|^2$  and  $|c_2(t)|^2$  and the local maximum of  $|c_3(t)|^2$ , respectively. A purple arrow (3) points the local minimum of  $|c_3(t)|^2$  that is found just before  $t = T_1/4$ , and its exact time is equal to  $t_{\min} = 510.82$ .

Now, we want to specify the time  $t$  when  $|c_1(t)|^2 \simeq |c_2(t)|^2 \simeq 1/2$  and  $|c_3(t)|^2 \simeq 0$  hold because we can obtain the maximally entangled state of  $|g\rangle_A|g\rangle_B$  and  $|e\rangle_A|e\rangle_B$  at this time.

Figures 1, 2, and 3 show graphs of  $|c_1(t)|^2$ ,  $|c_2(t)|^2$ , and  $|c_3(t)|^2$  as functions of time  $t$  with  $\omega_z = 10$  and  $\eta = 0.02$ , where  $c_1(t)$ ,  $c_2(t)$ , and  $c_3(t)$  are given by Eq. (32). In this case, the periods are given by  $T_1 = 2094.4$  and  $T_2^{(0)} = 44.429$ . From now on, when we carry out numerical calculations for concrete examples, we always set  $\omega_z$  and  $\eta$  to these values.

Looking at Figs. 1 and 2, we confirm that  $|c_1(t)|^2$  and  $|c_2(t)|^2$  form the beats with periods  $T_1$  and  $T_2^{(0)}$ . Amplitudes of the beats of  $|c_1(t)|^2$  and  $|c_2(t)|^2$  are nearly equal to  $1/2$  around  $t = T_1/4$ . Moreover,  $|c_3(t)|^2$  is a square of a sine wave with the period  $T_2^{(0)}$ . The graphs of Figs. 1, 2, and 3 are overlaid with each other in Fig. 4. Looking at Fig. 4, we can expect that  $|c_1(t)|^2 \simeq |c_2(t)|^2 \simeq 1/2$  and  $|c_3(t)|^2 \simeq 0$  hold around at  $t = T_1/4$ .

Figure 5 is an enlarged view of Fig. 4 near  $t = T_1/4 = 523.60$ . Numerical calculations tell us that we can find the local minimums of  $|c_1(t)|^2$  and  $|c_2(t)|^2$  at  $t = 521.89$  and  $t = 521.96$ , respectively. The nearest point where  $|c_3(t)|^2$  is locally maximum around  $t = T_1/4$  is  $t = 521.92$ . Thus, defining

$$t_{\min}^{(0)} = \left\lfloor \frac{T_1/4}{T_2^{(0)}/2} \right\rfloor \frac{T_2^{(0)}}{2}, \quad (38)$$

we can anticipate that  $|c_1(t)|^2 \simeq |c_2(t)|^2 \simeq 1/2$  and  $|c_3(t)|^2 \simeq 0$  near  $t = t_{\min}^{(0)}$ . In this case, it is given by  $t_{\min}^{(0)} = 510.93$ .

However, the actual time when  $|c_3(t)|^2$  becomes minimum just before  $t = T_1/4$  is given by  $t_{\min} = 510.82$  from numerical calculations of Eq. (32). Then, we obtain

$$\begin{aligned} c_1(t_{\min}) &= 0.480\,83 + 0.499\,63i \\ &\simeq e^{i\pi/4}/\sqrt{2}, \\ c_2(t_{\min}) &= -0.519\,17 + 0.499\,63i \\ &\simeq e^{i3\pi/4}/\sqrt{2}, \\ c_3(t_{\min}) &= 1.2966 \times 10^{-5} - 3.3804 \times 10^{-4}i. \end{aligned} \quad (39)$$

Here, we define the maximally entangled state of the ions A and B as

$$|\Psi\rangle_{AB} = \frac{e^{i\pi/4}}{\sqrt{2}}|g\rangle_A|g\rangle_B + \frac{e^{i3\pi/4}}{\sqrt{2}}|e\rangle_A|e\rangle_B. \quad (40)$$

Then, we obtain

$$|P\rangle\langle 0|_{AB}\langle\Psi|\psi(t_{\min})\rangle|^2 = 0.999\,63. \quad (41)$$

If we prepare the initial state  $|\psi(t=0)\rangle = |e, e, 0\rangle = (0, 1, 0)^T$  and describe its time evolution in the form

$$\begin{aligned} |\psi(t)\rangle &= U|\psi(0)\rangle \\ &= c'_1(t)|g, g, 0\rangle + c'_2(t)|e, e, 0\rangle + c'_3(t)|g, e, 1\rangle, \end{aligned} \quad (42)$$

the following relations hold for arbitrary time  $t$ :

$$\begin{aligned} c'_1(t) &\simeq c_2(t), \\ c'_2(t) &\simeq c_1(t), \\ c'_3(t) &\simeq c_3(t). \end{aligned} \quad (43)$$

## 5 The case where the initial state is prepared as $|g, g, 1\rangle$

We investigate the time evolution of the whole system's state that is initially prepared as  $|g, g, 1\rangle$ . We consider how to derive eigenvalues and eigenvectors of the Hamiltonian  $H$  that is given by Eq. (25) with  $n = 1$ . Rewriting the Hamiltonian as

$$H = \frac{1}{2}\eta\hbar\omega_z H', \quad (44)$$

we compute eigenvalues and eigenvectors approximately up to the first order of  $\eta$ . This treatment implies that we obtain approximations of eigenvalues up to the second order of  $\eta$  and those of eigenvectors up to the first order of  $\eta$ . Thus, we obtain

$$\begin{aligned} \lambda_1 &= 0, \\ \lambda_2 &= -\sqrt{6} + \frac{3}{2}\eta, \\ \lambda_3 &= \eta, \\ \lambda_4 &= \sqrt{6} + \frac{3}{2}\eta, \end{aligned} \quad (45)$$

$$\begin{aligned} \mathbf{v}_1 &= \frac{1}{\sqrt{2}}(-1, 1, 0, 0)^T, \\ \mathbf{v}_2 &= (i\tilde{r}(\eta), i\tilde{r}(\eta), \tilde{s}(\eta), \tilde{q}(\eta))^T, \\ \mathbf{v}_3 &= \frac{1}{\sqrt{3}}(-i\sqrt{2}\eta, -i\sqrt{2}\eta, 1, \sqrt{2})^T, \\ \mathbf{v}_4 &= (-i\tilde{r}(-\eta), -i\tilde{r}(-\eta), \tilde{s}(-\eta), \tilde{q}(-\eta))^T, \end{aligned} \quad (46)$$

where

$$\begin{aligned} \tilde{r}(\eta) &= \frac{1}{2} + \frac{1}{8}\sqrt{\frac{3}{2}}\eta, \\ \tilde{s}(\eta) &= -\frac{1}{\sqrt{3}} + \frac{11}{12\sqrt{2}}\eta, \\ \tilde{q}(\eta) &= \frac{1}{\sqrt{6}} + \frac{13}{24}\eta. \end{aligned} \quad (47)$$

Next, defining the following unitary operator

$$V = \begin{pmatrix} \mathbf{v}_1^\dagger \\ \mathbf{v}_2^\dagger \\ \mathbf{v}_3^\dagger \\ \mathbf{v}_4^\dagger \end{pmatrix}, \quad (48)$$

we can describe the unitary operator for the time evolution as

$$U = V^\dagger \begin{pmatrix} \exp(-i\tilde{\lambda}_1 t) & 0 & 0 & 0 \\ 0 & \exp(-i\tilde{\lambda}_2 t) & 0 & 0 \\ 0 & 0 & \exp(-i\tilde{\lambda}_3 t) & 0 \\ 0 & 0 & 0 & \exp(-i\tilde{\lambda}_4 t) \end{pmatrix} V, \quad (49)$$

where

$$\tilde{\lambda}_j = \frac{1}{2}\eta\omega_z\lambda_j \quad \text{for } j \in \{1, 2, 3, 4\}. \quad (50)$$

Setting the initial state to  $|\psi(t=0)\rangle = |g, g, 1\rangle = (1, 0, 0, 0)^T$ , we write the state at arbitrary time  $t$  as

$$\begin{aligned} |\psi(t)\rangle &= U|\psi(0)\rangle \\ &= \tilde{c}_1(t)|g, g, 1\rangle + \tilde{c}_2(t)|e, e, 1\rangle + \tilde{c}_3(t)|g, e, 2\rangle + \tilde{c}_4(t)|e, g, 0\rangle. \end{aligned} \quad (51)$$

To compute coefficients  $\tilde{c}_j(t)$  for  $j \in \{1, 2, 3, 4\}$ , we apply the following approximations to them. We leave factors  $\exp[-(i/2)\eta\omega_z\lambda_j t]$  for  $j \in \{1, 2, 3, 4\}$  untouched and calculate other factors and terms up to the first order of  $\eta$ . Furthermore, for  $\tilde{c}_3(t)$  and  $\tilde{c}_4(t)$ , we replace  $\exp[-(i/4)\eta(2\sqrt{6} + 3\eta)\omega_z t]$  and  $\exp[(i/4)\eta(2\sqrt{6} + \eta)\omega_z t]$  with  $\exp(-i\sqrt{3/2}\eta\omega_z t)$  and  $\exp(i\sqrt{3/2}\eta\omega_z t)$ , respectively. Based on the above approximations, we obtain

$$\begin{aligned} \tilde{c}_1(t) &\simeq \frac{1}{2} + \frac{1}{2}\exp(-i\frac{3}{4}\eta^2\omega_z t)[\cos(\frac{\sqrt{6}}{2}\eta\omega_z t) + i\frac{\sqrt{3}}{2\sqrt{2}}\sin(\frac{\sqrt{6}}{2}\eta\omega_z t)\eta], \\ \tilde{c}_2(t) &\simeq -1 + \tilde{c}_1(t), \\ \tilde{c}_3(t) &\simeq -\frac{1}{\sqrt{3}}\sin(\sqrt{\frac{3}{2}}\eta\omega_z t) - i\frac{\sqrt{2}}{3}[-1 + \cos(\sqrt{\frac{3}{2}}\eta\omega_z t)]\eta, \\ \tilde{c}_4(t) &\simeq -\frac{1}{\sqrt{2}}\tilde{c}_3(t) + i\eta[1 - \cos(\sqrt{\frac{3}{2}}\eta\omega_z t)]. \end{aligned} \quad (52)$$

From Eq. (52), we notice the following facts. The coefficient  $\tilde{c}_1(t)$  and  $\tilde{c}_2(t)$  form beats whose long and short periods are equal to  $T_1$  and  $T_2^{(1)}$ , where

$$T_2^{(1)} = \frac{2\sqrt{2}\pi}{\sqrt{3}\eta\omega_z}. \quad (53)$$

Thus, waves with the period  $T_1$  are the envelopes of the beats. The coefficients  $\tilde{c}_3(t)$  and  $\tilde{c}_4(t)$  become maximum or minimum at the same time. Hence,  $\tilde{c}_3(t)$  and  $\tilde{c}_4(t)$  approximately take the value zero at the same time.

Just before  $t = T_1/4 = 523.60$ ,  $|\tilde{c}_1(t)|^2$  and  $|\tilde{c}_2(t)|^2$  become locally minimum at  $t = 519.49$  and  $t = 519.38$ , respectively, and  $|\tilde{c}_3(t)|^2$  and  $|\tilde{c}_4(t)|^2$  become locally maximum at  $t = 519.43$  and  $t = 519.44$ , respectively. Thus, defining

$$t_{\min}^{(1)} = \left\lfloor \frac{T_1/4}{T_2^{(1)}/2} \right\rfloor \frac{T_2^{(1)}}{2}, \quad (54)$$

we can expect that  $|\tilde{c}_1(t)|^2 \simeq |\tilde{c}_2(t)|^2 \simeq 1/2$  and  $|\tilde{c}_3(t)|^2 \simeq |\tilde{c}_4(t)|^2 \simeq 0$  hold near at  $t = t_{\min}^{(1)}$ . In this case, it is given by  $t_{\min}^{(1)} = 513.02$ .

Remembering  $t_{\min} = 510.82$ , which is obtained as the optimized time in Sec. 4,  $\tilde{c}_j(t_{\min})$  for  $j \in \{1, 2, 3, 4\}$  are given by

$$\begin{aligned}\tilde{c}_1(t_{\min}) &= 0.513\,45 - 0.429\,19i, \\ \tilde{c}_2(t_{\min}) &= -0.486\,55 - 0.429\,19i, \\ \tilde{c}_3(t_{\min}) &= 0.011\,310 - 0.291\,41i, \\ \tilde{c}_4(t_{\min}) &= -0.008\,093\,4 + 0.215\,90i,\end{aligned}\quad (55)$$

and we obtain

$$|_{\mathbb{P}}\langle 1|_{\text{AB}}\langle \Psi|\psi(t_{\min})\rangle|^2 = 0.005\,194\,5. \quad (56)$$

Setting the initial state to  $|\psi(t=0)\rangle = |e, e, 1\rangle = (0, 1, 0, 0)^T$ , and describing the state of the whole system at arbitrary time  $t$  as

$$\begin{aligned}|\psi(t)\rangle &= U|\psi(0)\rangle \\ &= \tilde{c}'_1(t)|g, g, 1\rangle + \tilde{c}'_2(t)|e, e, 1\rangle + \tilde{c}'_3(t)|g, e, 2\rangle + \tilde{c}'_4(t)|e, g, 0\rangle,\end{aligned}\quad (57)$$

we obtain the following relations based on the above approximations:

$$\begin{aligned}\tilde{c}'_1(t) &\simeq \tilde{c}_2(t), \\ \tilde{c}'_2(t) &\simeq \tilde{c}_1(t), \\ \tilde{c}'_3(t) &\simeq \tilde{c}_3(t), \\ \tilde{c}'_4(t) &\simeq \tilde{c}_4(t).\end{aligned}\quad (58)$$

If we compute the time evolution of the system with the Hamiltonian given by Eq. (25)  $\forall n (\geq 1)$ , probabilities that we observe  $|g, g, n\rangle$  and  $|e, e, n\rangle$  form beats whose long and short periods are given by  $T_1$  and  $T_2^{(n)}$ , where

$$T_2^{(n)} = \frac{2\sqrt{2}\pi}{\sqrt{2n+1}\eta\omega_z}. \quad (59)$$

The probabilities that we observe  $|g, e, n+1\rangle$  and  $|e, g, n-1\rangle$  are represented by waves whose period is given by  $T_2^{(n)}$ .

## 6 Removing effects of thermal noise caused by fluctuation of the phonon mode

In this section, we investigate how to remove thermal noise for the case where the number of the phonons is equal to or less than one. That is to say, we consider a scenario where the thermal average number of phonons  $n_{\text{th}}$  increases from zero to a finite value because of the thermal distribution of the phonon mode. We examine a small perturbation from the ideal case of  $n_{\text{th}} = 0$ .

From Eq. (41), we become aware that we can obtain the maximally entangled state with very high fidelity if we choose the optimized time for the initial state  $|g, g, 0\rangle$ . However, from Eq. (56), we notice that the maximally entangled state is not always realized with high precision at this optimized time when the number of the phonons is equal to one. To overcome this problem, we apply an adjusted unitary transformation to the state where the number of the phonons is equal to one, so that the fidelity of the state and  $|\Psi\rangle$  defined by Eq. (40) becomes larger and the thermal effects are reduced.

Here, we define a unitary transformation  $R$  in the form

$$\begin{aligned} R|g\rangle_A|1\rangle_P &\rightarrow e^{-i\theta}|e\rangle_A|1\rangle_P, \\ R|e\rangle_A|1\rangle_P &\rightarrow e^{i\theta}|g\rangle_A|1\rangle_P, \\ R|j\rangle_A|0\rangle_P &\rightarrow |j\rangle_A|0\rangle_P \quad \text{for } j \in \{g, e\}. \end{aligned} \quad (60)$$

In Eq. (60), we do not deliberately define how the operator  $R$  works for the state  $|j\rangle_A|k\rangle_P$  for  $j \in \{g, e\}$  and  $k = 2, 3, \dots$ . Next, we define the fidelity of the state  $|\psi(t)\rangle$  and  $|\Psi\rangle_{AB}|1\rangle_P$  as

$$P(\theta) = |_P\langle 1|_{AB}\langle \Psi|R|\psi(t)\rangle|^2. \quad (61)$$

We assume that  $|\psi(t)\rangle$  have evolved from the initial state  $|\psi(0)\rangle = |g, g, 1\rangle$  until  $t_{\min} = 510.82$ . From numerical calculations, we find that  $P(\theta)$  is maximum at  $\theta = 0.075\,850$  and  $\theta = \pi + 0.075\,850$  and its maximum value is given by  $P(\theta) = 0.868\,57$ .

In contrast, the following relationship holds for the state  $|\psi(t)\rangle$  whose initial state is given by  $|\psi(t=0)\rangle = |g, g, 0\rangle$ ,

$$|_P\langle 0|_{AB}\langle \Psi|R|\psi(t)\rangle|^2 = |_P\langle 0|_{AB}\langle \Psi|\psi(t)\rangle|^2. \quad (62)$$

Based on these facts, we understand that the transformation  $R$  makes the operation of our proposed method robust and stable under the thermal fluctuation of the phonon mode. Next, we consider how to construct the unitary transformation  $R$ .

Here, we draw attention to the following facts. In this case,  $P(\theta)$  can take a relatively large value as the maximum. However, unfortunately, this scenario does not always happen. For example, if we set  $\eta = 0.015$ , the maximum value of  $P(\theta)$  is given by 0.653 49. The robustness of operations of our method relies on the maximum value of  $P(\theta)$  considerably and this is one of its drawbacks.

First of all, we consider the controlled-Z gate applied to the ion A and the phonon mode. We suppose an auxiliary level of the ion A,  $|e'\rangle_A$ , other than its original two levels  $\{|g\rangle_A, |e\rangle_A\}$  as shown in Fig. 6. We describe  $\omega_{\text{aux}}$  as an angular frequency that corresponds to the energy difference between the two levels  $|e'\rangle_A$  and  $|e\rangle_A$ . Applying a laser field whose net angular frequency and the Rabi frequency are given by  $\omega = \omega_{\text{aux}}$  and  $\Omega = -\omega_z/2$ , respectively, to the ion A, we obtain the Hamiltonian of the Jonathan–Plenio–Knight gate

$$H_I \simeq \frac{i}{2}\hbar\eta\omega_z(\sigma'_+a^\dagger - \sigma'_-a), \quad (63)$$

where  $\sigma'_\pm$  denote arising and lowering operators between the two levels  $\{|e'\rangle_A, |e\rangle_A\}$ .

The Hamiltonian  $H_I$  causes the following unitary transformation between the states  $\{|e'\rangle_A|0\rangle_P, |e\rangle_A|1\rangle_P\}$ . Here, we introduce a notation,  $|\tilde{0}\rangle = |e'\rangle_A|0\rangle_P$  and  $|\tilde{1}\rangle = |e\rangle_A|1\rangle_P$ .

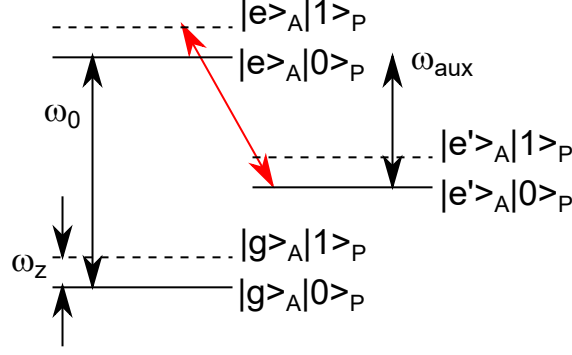


Figure 6: Energy levels for carrying out the controlled-Z gate.

Then, the following relations hold:

$$\begin{aligned} \sigma'_+ a^\dagger |\tilde{0}\rangle &= |\tilde{1}\rangle, & \sigma'_+ a^\dagger |\tilde{1}\rangle &= 0, \\ \sigma'_- a |\tilde{0}\rangle &= 0, & \sigma'_- a |\tilde{1}\rangle &= |\tilde{0}\rangle. \end{aligned} \quad (64)$$

Thus, defining the arising and lowering operators between the two states  $\{|\tilde{0}\rangle, |\tilde{1}\rangle\}$  as

$$J_+ = \sigma'_+ a^\dagger, \quad J_- = \sigma'_- a, \quad J_\pm = J_x \pm i J_y, \quad (65)$$

we rewrite the Hamiltonian as

$$\begin{aligned} H_I &= \frac{i}{2} \eta \hbar \omega_z (J_+ - J_-) \\ &= -\eta \hbar \omega_z J_y. \end{aligned} \quad (66)$$

Here, we define a unitary transformation

$$\begin{aligned} U &= \exp(-iH_I t/\hbar) \\ &= \exp(i\eta \omega_z t J_y). \end{aligned} \quad (67)$$

Setting the illumination time of the laser light to  $t = \pi/(\eta \omega_z)$ , we obtain the unitary matrix with basis vectors  $\{|\tilde{0}\rangle, |\tilde{1}\rangle\}$  as

$$U = \begin{pmatrix} -1 & 0 \\ 0 & -1 \end{pmatrix}, \quad (68)$$

where we use the following formula:

$$\exp\left(-\frac{i}{2} \theta \sigma_j\right) = \cos \frac{\theta}{2} \mathbf{I} - i \sin \frac{\theta}{2} \sigma_j \quad \text{for } j \in \{x, y, z\}. \quad (69)$$

The matrix  $U$  defined in Eq. (68) causes the following transformation:

$$\begin{aligned} |\tilde{0}\rangle &= |e'\rangle_A|0\rangle_P \longrightarrow -|\tilde{0}\rangle = -|e'\rangle_A|0\rangle_P, \\ |\tilde{1}\rangle &= |e\rangle_A|1\rangle_P \longrightarrow -|\tilde{1}\rangle = -|e\rangle_A|1\rangle_P. \end{aligned} \quad (70)$$

This transformation implies that basis vectors  $|g\rangle_A|0\rangle_P$ ,  $|g\rangle_A|1\rangle_P$  and  $|e\rangle_A|0\rangle_P$  are left untouched and only a transition  $|e\rangle_A|1\rangle_P \rightarrow -|e\rangle_A|1\rangle_P$  occurs. We can describe this operation as a matrix with basis vectors  $\{|g\rangle_A|0\rangle_P, |g\rangle_A|1\rangle_P, |e\rangle_A|0\rangle_P, |e\rangle_A|1\rangle_P\}$  in the form

$$C(Z)_{AP} = \begin{pmatrix} 1 & 0 & 0 & 0 \\ 0 & 1 & 0 & 0 \\ 0 & 0 & 1 & 0 \\ 0 & 0 & 0 & -1 \end{pmatrix}, \quad (71)$$

and finally we obtain the controlled-Z gate.

Next, we consider a one-qubit rotation applied to the ion A. Taking the basis vectors  $\{|g\rangle_A, |e\rangle_A\}$ , we define the following unitary transformation:

$$V_A(\phi) = \frac{1}{\sqrt{2}} \begin{pmatrix} e^{i\phi} & 1 \\ -1 & e^{-i\phi} \end{pmatrix}. \quad (72)$$

Then, we obtain a relation

$$V_A(\phi)\sigma_{Az}V_A^\dagger(\phi) = - \begin{pmatrix} 0 & e^{i\phi} \\ e^{-i\phi} & 0 \end{pmatrix}, \quad (73)$$

and we can decompose the operator  $R$  as

$$R = V_A(\pi + \theta)C(Z)_{AP}V_A^\dagger(\pi + \theta). \quad (74)$$

Next, we investigate implementation of  $V_A(\phi)$ . Here, we remember the following fact. According to the prescription of the Jonathan–Plenio–Knight gate, the basis vectors  $\{|0\rangle_A, |1\rangle_A\}$  are converted into  $\{| \pm \rangle_A\}$ . Thus, the unitary transformation  $V_A(\phi)$  defined in Eq. (72) must be replaced with  $\tilde{R}_A V_A(\phi) \tilde{R}_A^\dagger$  and  $V_A(\phi)$  must be regarded as a rotation between  $|0\rangle_A$  (the ground state of the ion A) and  $|1\rangle_A$  (the excited state of the ion A), where  $\tilde{R}$  is defined in Eq. (11).

Moreover, we draw attention to the following points. The ion trap quantum computer can carry out one-qubit rotations around the  $x$ - and  $y$ -axes with ease but it can hardly perform those around the  $z$ -axis. Thus, we better decompose  $V_A(\phi)$  into a combination of rotations around the  $x$ - and  $y$ -axes. Here, we define the following three unitary rotations:

$$R_{Al}(\alpha) = \exp\left(-\frac{i}{2}\alpha\sigma_{Al}\right) \quad \text{for } l \in \{x, y, z\}. \quad (75)$$

For example, the operator  $\tilde{R}$  defined in Eq. (11) is rewritten in the form  $\tilde{R}_A = R_{Ay}(-\pi/2)$ . The operator  $V_A(\phi)$  is decomposed into one-qubit rotations around  $x$ - and  $y$ -axes as

$$V_A(\phi) = R_{Az}(-\phi)R_{Ay}(-\frac{\pi}{2})R_{Az}(-\phi), \quad (76)$$

$$R_{Az}(-\phi) = R_{Ax}(\frac{\pi}{2})R_{Ay}(-\phi)R_{Ax}(-\frac{\pi}{2}). \quad (77)$$

We can carry out the one-qubit rotation around the  $x$ -axis as follows. Applying the laser light with  $\delta = 0$ , that is to say, with the angular frequency  $\omega = \omega_0$ , and eliminate

the terms  $\exp(\pm i\omega_z t)$  according to the rotating wave approximation, we can rewrite the Hamiltonian  $H'_I$  given by Eq. (8) as

$$\begin{aligned} H'_I &\simeq \hbar\Omega(\sigma_+ + \sigma_-) \\ &= 2\hbar\Omega\sigma_x. \end{aligned} \quad (78)$$

This Hamiltonian realizes  $R_x(\alpha)$ .

The Hamiltonian of Eq. (8) is induced by the magnetic flux density that is a uniform wave propagating along the  $z$  direction and being polarized in the  $x$  direction. Thus, to realize the rotation  $R_y(\alpha)$ , we apply the magnetic flux density propagating along the  $z$  direction and being polarized in the  $y$  direction to the ion.

These arguments are valid for the four-dimensional Hilbert space spanned by the basis vectors  $\{|g\rangle_A|0\rangle_P, |g\rangle_A|1\rangle_P, |e\rangle_A|0\rangle_P, |e\rangle_A|1\rangle_P\}$  of the ion A and the phonon mode. However, the actual whole Hilbert space of the system contains the other basis vectors,  $|g\rangle_A|n\rangle_P, |e\rangle_A|n\rangle_P$  for  $n = 2, 3, \dots$ . Thus, for example, the Hamiltonian given by Eq. (63) causes a rotation between states  $|e\rangle_A|2\rangle_P$  and  $|e'\rangle_A|1\rangle_P$ . Hence, if we define  $P'(\theta)$  with the transformation  $R$  given by Eq. (60) as

$$P'(\theta) = |_P\langle 2|_{AB}\langle\Psi|R|\psi(t)\rangle|^2, \quad (79)$$

where  $|\psi(0)\rangle = |g, g, 2\rangle$ , the parameter  $\theta$  that maximized  $P'(\theta)$  is not equal to the parameter  $\theta$  that maximizes  $P(\theta)$  defined in Eq. (61) in general. Here, we define fidelities

$$\mathcal{F}^{(m)} = \sum_{n=0}^m p_n |_P\langle n|_{AB}\langle\Psi|R|\psi_n(t)\rangle|^2 \quad \text{for } m = 1, 2, \dots, \quad (80)$$

$$\mathcal{F}^{(m)} \leq \mathcal{F}^{(\infty)}, \quad (81)$$

where  $p_n$  represents the probability that the number of phonons is equal to  $n$  according to the Bose–Einstein statics, and  $|\psi_n(t)\rangle$  denotes the state at the arbitrary time  $t$  which is initially prepared as  $|g, g, n\rangle$  at  $t = 0$ . Then, we assume that the parameter  $\theta$  maximizes  $P(\theta)$ . This  $\theta$  only maximizes  $\mathcal{F}^{(1)}$  but does not maximizes  $\mathcal{F}^{(n)}$  for  $n = 2, 3, \dots$ .

## 7 Comparisons among operation times of the quantum gates

In this section, we make comparisons among operation times of the Cirac–Zoller gate, the Jonathan–Plenio–Knight gate, and the proposed gate.

First, we consider Cirac and Zoller’s method. We apply laser light with a net angular frequency  $\omega = \omega_0$  and the Rabi frequency  $\Omega$  to the ion for carrying out the one-qubit gate. Thus, its coupling constant appearing in the Hamiltonian is given by  $\Omega$ . Contrastingly, to perform the ion–phonon quantum gate, we let laser light with a net angular frequency  $\omega = \omega_0 - \omega_z$  and the Rabi frequency  $\Omega$  illuminates the ion. Thus, its coupling constant appearing in the Hamiltonian is given by  $\eta\Omega$ . To execute the one-qubit and ion–phonon

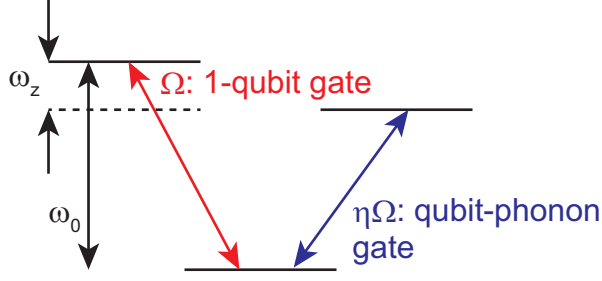


Figure 7: A schematic of energy levels for Cirac and Zoller's one-qubit and ion-phonon gates.

gates stably, two processes shown in Fig. 7 must be distinguishable from each other. Thus, we obtain a condition

$$\Omega\eta \ll \omega_z. \quad (82)$$

Hence, describing operation times of Cirac and Zoller's one-qubit and ion-phonon gates as  $\tau_{\text{CZ1}}$  and  $\tau_{\text{CZ2}}$ , respectively, we obtain

$$\tau_{\text{CZ1}} \sim \Omega^{-1}, \quad \tau_{\text{CZ2}} \sim (\eta\Omega)^{-1}, \quad \tau_{\text{CZ2}} \gg \tau_{\text{CZ1}}, \quad (83)$$

$$\tau_{\text{CZ2}} \gg \omega_z^{-1}. \quad (84)$$

Equation (84) implies that the operation time for generating entanglement with Cirac and Zoller's ion-phonon quantum gate is much longer than  $\omega_z^{-1}$ .

We have obtained Eq. (82) as the condition of Cirac and Zoller's ion-phonon quantum gate. However, this condition becomes useless as  $\eta \rightarrow 0$ . To overcome this problem, we return to the original Hamiltonian of Cirac and Zoller's ion-phonon quantum gate. If we apply a laser field with  $\delta = -\omega_z$ , that is to say, with a frequency  $\omega = \omega_0 - \omega_z$  to the ion, the Hamiltonian defined in Eq. (8) is rewritten in the form under  $\eta \rightarrow 0$

$$H'_I = \hbar\Omega[\sigma_+ \exp(i\omega_z t) + \sigma_- \exp(-i\omega_z t)]. \quad (85)$$

Assuming that the initial state of the ion A and the phonon mode P is given by  $|g\rangle_A|0\rangle_P$ , we evaluate the correction of the energy with the perturbation theory. We obtain the first-order energy shift as

$${}_{\text{A}}\langle g|_P\langle 0|H'_I|g\rangle_A|0\rangle_P = 0. \quad (86)$$

The second-order energy shift is given by

$$-\sum_{m \neq 0} \frac{|\langle\psi_m|H'_I|\psi_0\rangle|^2}{E_m - E_0}, \quad (87)$$

where  $|\psi_0\rangle$  denotes the initial state,  $E_0$  represents the energy level of  $|\psi_0\rangle$ ,  $|\psi_m\rangle$  denotes the intermediate state, and  $E_m$  represents the energy level of  $|\psi_m\rangle$ . Substitutions of the

initial state  $|\psi_0\rangle = |g\rangle_A|0\rangle_P$ , the energy of the laser field  $E_0 = \hbar(\omega_0 - \omega_z)$ , the intermediate state  $|\psi_m\rangle = |e\rangle_A|0\rangle_P$ , and the excitation energy of the ion  $E_m = \hbar\omega_0$  into Eq. (87) gives the second-order energy shift in the form

$$-\hbar \frac{|\Omega \exp(i\omega_z t)|^2}{\omega_z} = -\frac{\hbar\Omega^2}{\omega_z}. \quad (88)$$

To assure that the quantum gate works correctly, we must let the second-order correction of the energy be much smaller than the product of the coupling constant  $\eta\Omega$  and  $\hbar$ . Thus, we obtain another condition

$$\Omega \ll \eta\omega_z. \quad (89)$$

This condition is stricter than that of Eq. (82). Thus, we attain

$$\tau_{\text{CZ2}} \gg \frac{1}{\eta^2\omega_z}. \quad (90)$$

We use the following three quantum gates in our proposal. The first one is the quantum gate that generates entanglement between the two ions A and B using the laser light with the net angular frequency  $\omega = \omega_0$  and the Rabi frequency  $\Omega = \pm\omega_z/2$ . The operation time of this quantum gate is around  $T_1$  given by Eq. (36) and on the order of  $(\eta^2\omega_z)^{-1}$ . The second one is the controlled-Z gate implemented with the laser field of the net angular frequency  $\omega = \omega_{\text{aux}}$  and the Rabi frequency  $\Omega = -\omega_z/2$ . The operation time is on the order of  $(\eta\omega_z)^{-1}$  because of Eq. (67). The third one is the one-qubit rotation that is introduced by Cirac and Zoller's method. To carry out this gate, we apply the laser field of the net angular frequency  $\omega = \omega_0$  and the Rabi frequency  $\Omega$ , where  $\Omega$  must obey the condition of Eq. (89). Thus, the operation time is given by  $\tau_{\text{CZ1}}$ . These operation times are much smaller than that of Cirac and Zoller's ion-phonon gate due to Eq. (90).

In contrast, the operation time of Jonathan, Plenio, and Knight's ion-phonon gate is on the order of  $(\eta\omega_z)^{-1}$ . Thus, the switching rate of our process is lower than that of Jonathan, Plenio, and Knight's method.

Therefore, we can conclude that our method is superior to Cirac and Zoller's method in terms of the speed of the operation.

## 8 Numerical simulations of thermal motion of the proposed gate

In this section, carrying out numerical simulations, we confirm that the proposed gate works stably even if the mean phonon number in thermal equilibrium is larger than zero.

First, we use  $H$  defined in Eq. (22) as the Hamiltonian of the whole system. For the numerical calculations, we consider the Hilbert space in which the number of phonons is less than or equal to 14, so that it is 60-dimensional in total.

We assume that the phonons obey the Bose-Einstein statistics. Thus, the probability that the number of phonons is equal to  $n$  is given by

$$p_n = [1 - \exp(-\beta\hbar\omega_z)] \exp(-\beta\hbar n\omega_z), \quad (91)$$

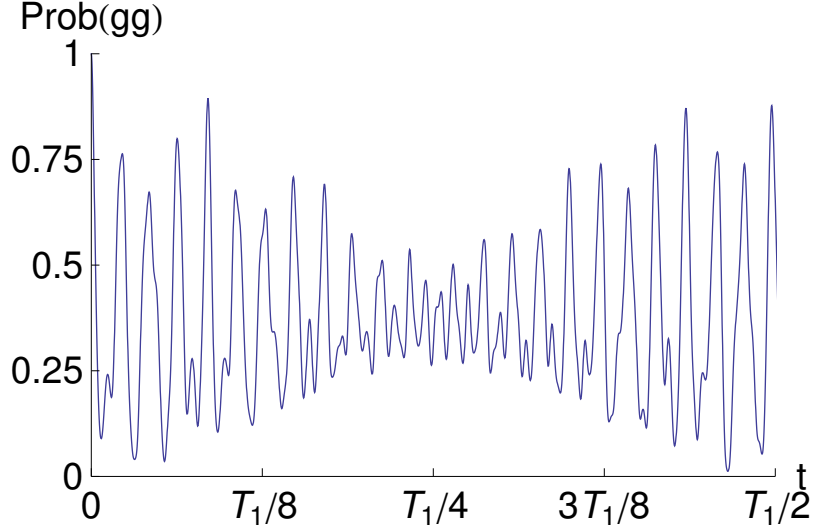


Figure 8: A graph of a probability that we can observe  $|g\rangle_A|g\rangle_B$  in the proposed process as a function of time with  $\omega_z = 10$ ,  $\eta = 0.02$ , and  $n_{\text{th}} = 0.5$ . We can regard this curve as that of Fig. 1 suffering from the thermal noise.

where  $T$  denotes the temperature,  $k_B$  represents the Boltzmann constant, and  $\beta = 1/(k_B T)$ . The mean phonon number in thermal equilibrium is given in the form

$$n_{\text{th}} = [\exp(\beta \hbar \omega_z) - 1]^{-1}. \quad (92)$$

From the results given in Secs. 4 and 5, we set  $\omega_z = 10$  and  $\eta = 0.02$ , and we choose the time  $t_{\text{min}} = 510.82$  for obtaining the maximally entangled state. Letting the time be constant as  $t_{\text{min}} = 510.82$  and varying value of  $n_{\text{th}}$ , we examine how fidelities  $\mathcal{F}$  and  $\mathcal{F}^{(1)}$  depend on  $n_{\text{th}}$ , where  $\mathcal{F}$  is defined as

$$\mathcal{F} = \sum_{n=0}^{\infty} p_n |_{\text{P}} \langle n |_{\text{AP}} \langle \Psi | \psi_n(t) \rangle |^2. \quad (93)$$

Figures 8, 9, and 10 show probabilities that we observe states  $|g\rangle_A|g\rangle_B$ ,  $|e\rangle_A|e\rangle_B$ ,  $|g\rangle_A|e\rangle_B$ , and  $|e\rangle_A|g\rangle_B$  as functions of time during our process under thermal noise with  $n_{\text{th}} = 0.5$ . We can regard Figs. 8 and 9 as versions of Figs. 1 and 2 suffering from thermal fluctuation.

Figure 11 shows graphs of  $\mathcal{F}$  and  $\mathcal{F}^{(1)}$  as functions of  $n_{\text{th}}$  for  $t_{\text{min}} = 510.82$ . Looking at Fig. 11, we note that  $\mathcal{F} \leq \mathcal{F}^{(1)}$  holds for  $0 \leq n_{\text{th}} \leq 1.38$  and the transformation  $R$  is useful for reducing the thermal noise in this range. Moreover, this graph indicates that  $\mathcal{F}^{(1)} \geq 0.950$  holds for  $0 \leq n_{\text{th}} \leq 0.200$ . Referring to Ref. [19],  ${}^9\text{Be}^+$  ions in a trap allows us a typical frequency of phonons  $\omega_z/(2\pi) = 10$  MHz. If we set  $n_{\text{th}} = 0.200$  and  $\omega_z/(2\pi) = 10$  MHz, we obtain

$$\begin{aligned} T &= \frac{\hbar \omega_z}{k_B} [\log(1 + \frac{1}{n_{\text{th}}})]^{-1} \\ &= 0.558 \hbar \omega_z / k_B \\ &= 2.68 \times 10^{-4} \text{ K}. \end{aligned} \quad (94)$$

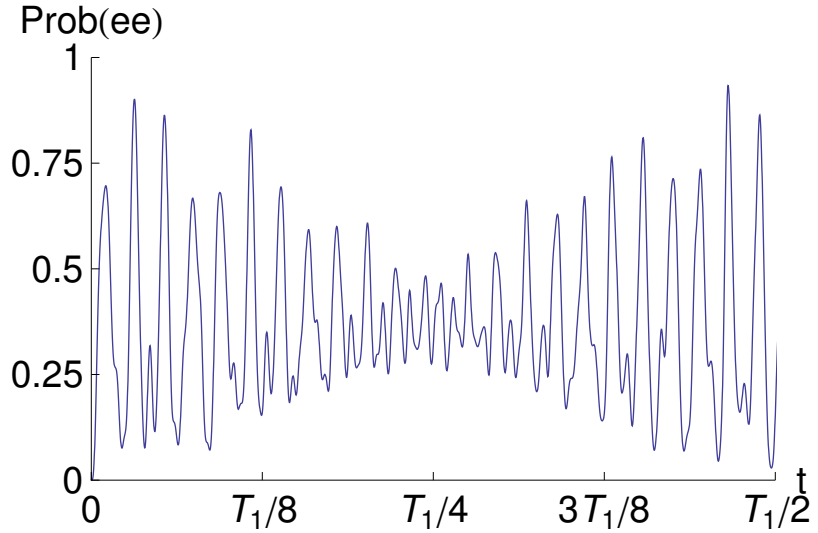


Figure 9: A graph of a probability that we can observe  $|e\rangle_A|e\rangle_B$  in the proposed process as a function of time with  $\omega_z = 10$ ,  $\eta = 0.02$ , and  $n_{\text{th}} = 0.5$ . We can regard this curve as that of Fig. 2 suffering from the thermal noise.

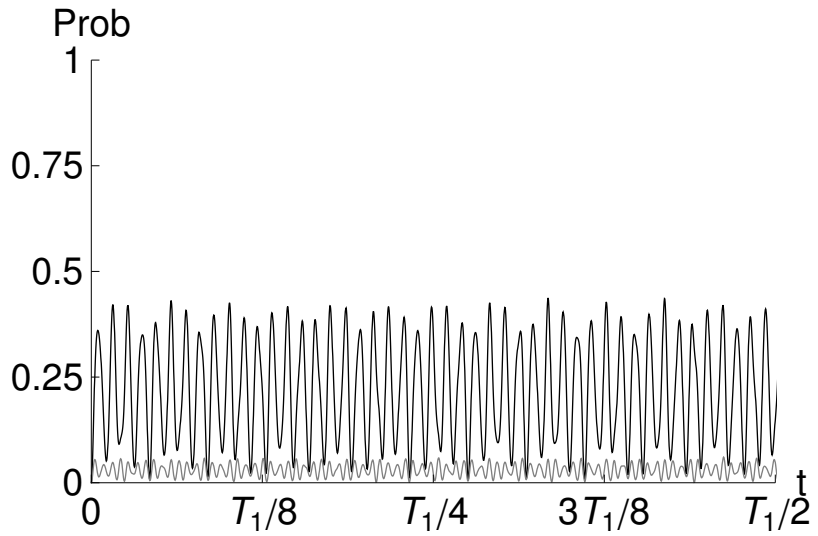


Figure 10: Graphs of probabilities that we can observe  $|g\rangle_A|e\rangle_B$  and  $|e\rangle_A|g\rangle_B$  for the process we proposed as functions of time with  $\omega_z = 10$ ,  $\eta = 0.02$ , and  $n_{\text{th}} = 0.5$ . The black and grey curves represent  $|g\rangle_A|e\rangle_B$  and  $|e\rangle_A|g\rangle_B$ , respectively.

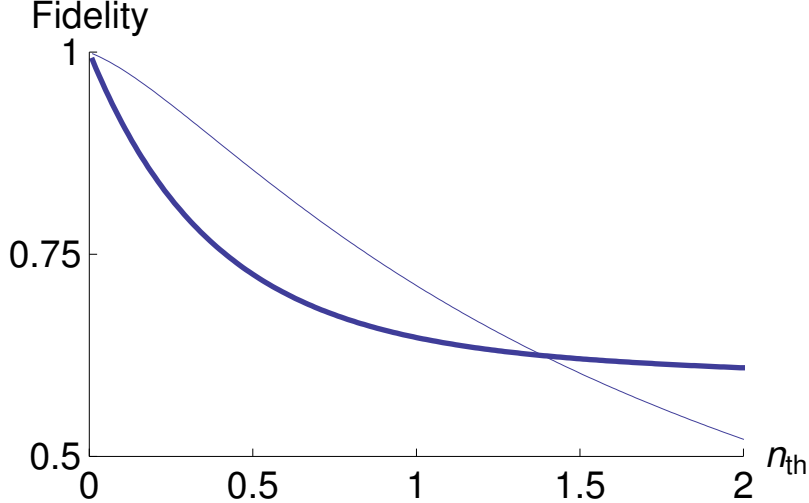


Figure 11: Graphs of  $\mathcal{F}$  and  $\mathcal{F}^{(1)}$  as functions of  $n_{\text{th}}$  with  $\omega_z = 10$  and  $\eta = 0.02$ , and the time  $t_{\text{min}} = 510.82$ . The thick and thin curves represent  $\mathcal{F}$  and  $\mathcal{F}^{(1)}$ , respectively. If  $n_{\text{th}} = 0.200$ , we obtain  $\mathcal{F} = 0.846$  and  $\mathcal{F}^{(1)} = 0.951$ . In the range of  $0 \leq n_{\text{th}} \leq 1.38$ ,  $\mathcal{F} \leq \mathcal{F}^{(1)}$  holds and we can consider that the transformation  $R$  enlarges the fidelity effectively.

As another example, referring to Ref. [9],  $^{40}\text{Ca}^+$  ions in a trap give us  $\omega_z/(2\pi) = 1.7$  MHz. In this case, setting  $n_{\text{th}} = 0.200$ , we obtain  $T = 4.55 \times 10^{-5}$  K.

Generally, the ion trap quantum computer is cooled to the temperature  $k_B T \ll \hbar\omega_z$  by the sideband cooling method. By contrast, our method allows the ion trap quantum computer to work at a higher temperature than the conventional one. This is a remarkable advantage of our method.

## 9 Discussions

An attempt to let the Jonathan–Plenio–Knight gate not be vulnerable to the thermal phonon mode was made in Ref. [24]. In Ref. [24], two ions are illuminated simultaneously with a single laser field that is resonant with the excitation energy of the ions, that is to say,  $\hbar\omega_0$ . The method shown in Ref. [24] and ours are similar on this point. However, our method requires two laser fields that have a phase difference of  $\pi$  and are applied to the two ions individually. This is a difference between the two methods. In the case of Ref. [24], the Hamiltonian of the interaction is given by

$$H'_{\text{eff}} \approx -\hbar\omega[|eg\rangle\langle ge| + |ge\rangle\langle eg|], \quad (95)$$

$$\omega = \frac{\Omega^2}{2} \sum_{p=1}^2 \frac{\eta_{1p}\eta_{2p}\nu_p}{\Omega^2 - \nu_p^2}, \quad (96)$$

where  $\Omega$  denotes the Rabi frequency of the laser light, the centre-of-mass mode and the second collective mode (the ‘breathing’ mode) are represented by  $p = 1$  and  $p = 2$ ,

respectively,  $\eta_{jp}$  ( $j \in \{1, 2\}$ ,  $p \in \{1, 2\}$ ) denotes an ‘effective’ Lamb–Dicke parameter incorporating the relative displacement of the  $j$ th ion in the  $p$ th mode, and  $\nu_p$  represents the frequency of the  $p$ th collective mode phonon (for example,  $\nu_1 = \omega_z$ ). If we set  $\eta_{1p} = \eta_{2p} = \eta$  for  $p \in \{1, 2\}$ , use a relationship  $\Omega = 1.5\nu_1$  as shown in concrete numerical calculations of Ref. [24], and let  $\nu_1 = \nu_2 = \omega_z$  hold, we obtain  $\omega \propto \eta^2 \omega_z$ .

Thus, the operation time for generating the maximally entangled state with the Hamiltonian  $H'_{\text{eff}}$  given by Eq. (95) is on the order of  $(\eta^2 \omega_z)^{-1}$ . This operation time is nearly equal to that of our method. Hence, there is no essential difference between the two methods concerning the operation time. However, Ref. [24] required slightly difficult time-averaging arguments [25] for deriving time-independent effective Hamiltonian and it was a disadvantage for the general audience. Thus, our method is superior to that of Ref. [24] because of this point.

In this paper, we obtain the upper limit of  $n_{\text{th}}$  as  $n_{\text{th}} = 0.200$  for the concrete example. This value relaxes the restriction of the temperature of ions considerably in the actual experiments.

For the linear ion trap, the sideband cooling method is used to cool ions. Reference [26] reported that Cs atoms in a two-dimensional optical lattice were cooled along  $x$ - and  $y$ -axes by the sideband cooling method and the average numbers of thermal phonons reached  $\bar{n}_x \approx \bar{n}_y < 0.024$ . Reference [27] reported that a chain of 25 ions of  $^{171}\text{Yb}^+$  were cooled by the sideband cooling method, individual ions were used to cool individual motional modes in parallel, and almost all of the modes of motion were cooled to below 0.2 quanta except for four ions reaching about 0.5 quanta.

Reference [28] concluded that the Doppler cooling method could cool ions below the temperature of a few mK. In this paper, we estimate the upper limit of the temperature for  $^9\text{Be}^+$  ion at 0.268 mK. Thus, this limit is very close to the temperature attained by the Doppler cooling method.

In this paper, we investigate the extension of the Jonathan–Plenio–Knight gate and examine how to obtain the maximally entangled state with high fidelity at the temperature where the average number of thermal phonons is less than one but not equal to zero. The proposed method considerably relaxes the restriction of low temperature that must be attained by the sideband cooling method for the initial state of the ion trap quantum computer. The operation time of our method is shorter in comparison with operation times of the Cirac–Zoller and Mølmer–Sørensen gates.

Reference [29] insisted that there were no theoretical limitations for the speed of the two-qubit gate in the ion trap quantum computer. However, Ref. [29] did not show actual implementation for realizing the two-qubit gate that worked in an arbitrarily short time. Thus, exploration of new ideas on how to realize a fast two-qubit gate for the ion trap quantum computer is very challenging and interesting.

The switching rate of our scheme is lower than that of the Jonathan–Plenio–Knight gate. Hence, we can regard our method as a compromise solution for insensitivity to the thermal motion and the high-speed operation. However, we think that this solution will become very practical in the future.

## Acknowledgements

This work was supported by MEXT Quantum Leap Flagship Program (MEXT Q-LEAP) Grant Number JPMXS0120351339.

## Data availability statement

The data obtained by numerical calculations and C++ programs will be available from the author upon reasonable request.

## References

- [1] J. Preskill, ‘Quantum computing in the NISQ era and beyond’, *Quantum* **2**, 79 (2018). [doi:10.22331/q-2018-08-06-79](https://doi.org/10.22331/q-2018-08-06-79)
- [2] F. Arute, K. Arya, R. Babbush, D. Bacon, J. C. Bardin, R. Barends, R. Biswas, S. Boixo, F. G. S. L. Brandao, D. A. Buell, B. Burkett, Y. Chen, Z. Chen, B. Chiaro, R. Collins, W. Courtney, A. Dunsworth, E. Farhi, B. Foxen, A. Fowler, C. Gidney, M. Giustina, R. Graff, K. Guerin, S. Habegger, M. P. Harrigan, M. J. Hartmann, A. Ho, M. Hoffmann, T. Huang, T. S. Humble, S. V. Isakov, E. Jeffrey, Z. Jiang, D. Kafri, K. Kechedzhi, J. Kelly, P. V. Klimov, S. Knysh, A. Korotkov, F. Kostritsa, D. Landhuis, M. Lindmark, E. Lucero, D. Lyakh, S. Mandrà, J. R. McClean, M. McEwen, A. Megrant, X. Mi, K. Michelsen, M. Mohseni, J. Mutus, O. Naaman, M. Neeley, C. Neill, M. Y. Niu, E. Ostby, A. Petukhov, J. C. Platt, C. Quintana, E. G. Rieffel, P. Roushan, N. C. Rubin, D. Sank, K. J. Satzinger, V. Smelyanskiy, K. J. Sung, M. D. Trevithick, A. Vainsencher, B. Villalonga, T. White, Z. J. Yao, P. Yeh, A. Zalcman, H. Neven, and J. M. Martinis, ‘Quantum supremacy using a programmable superconducting processor’, *Nature* **574**(7779), 505–510 (2019). [doi:10.1038/s41586-019-1666-5](https://doi.org/10.1038/s41586-019-1666-5)
- [3] J. Koch, T. M. Yu, J. Gambetta, A. A. Houck, D. I. Schuster, J. Majer, A. Blais, M. H. Devoret, S. M. Girvin, and R. J. Schoelkopf, ‘Charge-insensitive qubit design derived from the Cooper pair box’, *Phys. Rev. A* **76**(4), 042319 (2007). [doi:10.1103/PhysRevA.76.042319](https://doi.org/10.1103/PhysRevA.76.042319)
- [4] E. Knill, R. Laflamme, and G. J. Milburn, ‘A scheme for efficient quantum computation with linear optics’, *Nature* **409**(6816), 46–52 (2001). [doi:10.1038/35051009](https://doi.org/10.1038/35051009)
- [5] R. Raussendorf, D. E. Browne, and H. J. Briegel, ‘Measurement-based quantum computation on cluster states’, *Phys. Rev. A* **68**(2), 022312 (2003). [doi:10.1103/PhysRevA.68.022312](https://doi.org/10.1103/PhysRevA.68.022312)
- [6] M. Khazali and K. Molmer, ‘Fast multiqubit gates by adiabatic evolution in interacting excited-state manifolds of rydberg atoms and superconducting circuits’, *Phys. Rev. X* **10**(2), 021054 (2020). [doi:10.1103/PhysRevX.10.021054](https://doi.org/10.1103/PhysRevX.10.021054)

- [7] N. Friis, O. Marty, C. Maier, C. Hempel, M. Holzäpfel, P. Jurcevic, M. B. Plenio, M. Huber, C. Roos, R. Blatt, and B. Lanyon, ‘Observation of entangled states of a fully controlled 20-qubit system’, *Phys. Rev. X* **8**(2), 021012 (2018). [doi:10.1103/PhysRevX.8.021012](https://doi.org/10.1103/PhysRevX.8.021012)
- [8] J. I. Cirac and P. Zoller, ‘Quantum computations with cold trapped ions’, *Phys. Rev. Lett.* **74**(20), 4091–4094 (1995). [doi:10.1103/PhysRevLett.74.4091](https://doi.org/10.1103/PhysRevLett.74.4091)
- [9] S. Gulde, M. Riebe, G. P. T. Lancaster, C. Becher, J. Eschner, H. Häffner, F. Schmidt-Kaler, I. L. Chuang, and R. Blatt, ‘Implementation of the Deutsch–Jozsa algorithm on an ion-trap quantum computer’, *Nature* **421**(6918), 48–50 (2003). [doi:10.1038/nature01336](https://doi.org/10.1038/nature01336)
- [10] D. Kielpinski, C. Monroe, and D. J. Wineland, ‘Architecture for a large-scale ion-trap quantum computer’, *Nature* **417**(6890), 709–711 (2002). [doi:10.1038/nature00784](https://doi.org/10.1038/nature00784)
- [11] Y. Wang, M. Um, J. Zhang, S. An, M. Lyu, J.-N. Zhang, L.-M. Duan, D. Yum, and K. Kim, ‘Single-qubit quantum memory exceeding ten-minute coherence time’, *Nat. Photonics* **11**(10), 646–650 (2017). [doi:10.1038/s41566-017-0007-1](https://doi.org/10.1038/s41566-017-0007-1)
- [12] A. H. Myerson, D. J. Szwer, S. C. Webster, D. T. C. Allcock, M. J. Curtis, G. Imreh, J. A. Sherman, D. N. Stacey, A. M. Steane, and D. M. Lucas, ‘High-fidelity readout of trapped-ion qubits’, *Phys. Rev. Lett.* **100**(20), 200502 (2008). [doi:10.1103/PhysRevLett.100.200502](https://doi.org/10.1103/PhysRevLett.100.200502)
- [13] T. P. Harty, D. T. C. Allcock, C. J. Ballance, L. Guidoni, H. A. Janacek, N. M. Linke, D. N. Stacey, and D. M. Lucas, ‘High-fidelity preparation, gates, memory, and readout of a trapped-ion quantum bit’, *Phys. Rev. Lett.* **113**(22), 220501 (2014). [doi:10.1103/PhysRevLett.113.220501](https://doi.org/10.1103/PhysRevLett.113.220501)
- [14] J. P. Gaebler, T. R. Tan, Y. Lin, Y. Wan, R. Bowler, A. C. Keith, S. Glancy, K. Coakley, E. Knill, D. Leibfried, and D. J. Wineland, ‘High-fidelity universal gate set for  ${}^9\text{Be}^+$  ion qubits’, *Phys. Rev. Lett.* **117**(6), 060505 (2016). [doi:10.1103/PhysRevLett.117.060505](https://doi.org/10.1103/PhysRevLett.117.060505)
- [15] C. J. Ballance, T. P. Harty, N. M. Linke, M. A. Sepiol, and D. M. Lucas, ‘High-fidelity quantum logic gates using trapped-ion hyperfine qubits’, *Phys. Rev. Lett.* **117**(6), 060504 (2016). [doi:10.1103/PhysRevLett.117.060504](https://doi.org/10.1103/PhysRevLett.117.060504)
- [16] N. Grzesiak, R. Blümel, K. Wright, K. M. Beck, N. C. Pisenti, M. Li, V. Chaplin, J. M. Amini, S. Debnath, J.-S. Chen, and Y. Nam, ‘Efficient arbitrary simultaneously entangling gates on a trapped-ion quantum computer’, *Nat. Commun.* **11**, 2963 (2020). [doi:10.1038/s41467-020-16790-9](https://doi.org/10.1038/s41467-020-16790-9)
- [17] M. A. Nielsen and I. L. Chuang, *Quantum computation and quantum information* (Cambridge University Press, Cambridge, U.K., 2002).
- [18] A. Steane, ‘The ion trap quantum information processor’, *Appl. Phys. B* **64**(6), 623–643 (1997). [doi:10.1007/s003400050225](https://doi.org/10.1007/s003400050225)

- [19] D. J. Wineland, C. Monroe, W. M. Itano, D. Leibfried, B. E. King, and D. M. Meekhof, ‘Experimental issues in coherent quantum-state manipulation of trapped atomic ions’, *J. Res. Natl. Inst. Stand. Technol.* **103**(3), 259–328 (1998). [doi:10.6028/jres.103.019](https://doi.org/10.6028/jres.103.019)
- [20] C. D. Bruzewicz, J. Chiaverini, R. McConnell, and J. M. Sage, ‘Trapped-ion quantum computing: progress and challenges’, *Appl. Phys. Rev.* **6**(2), 021314 (2019). [doi:10.1063/1.5088164](https://doi.org/10.1063/1.5088164)
- [21] D. Jonathan, M. B. Plenio, and P. L. Knight, ‘Fast quantum gates for cold trapped ions’, *Phys. Rev. A* **62**(4), 042307 (2000). [doi:10.1103/PhysRevA.62.042307](https://doi.org/10.1103/PhysRevA.62.042307)
- [22] K. Mølmer and A. Sørensen, ‘Multiparticle entanglement of hot trapped ions’, *Phys. Rev. Lett.* **82**(9), 1835–1838 (1999). [doi:10.1103/PhysRevLett.82.1835](https://doi.org/10.1103/PhysRevLett.82.1835)
- [23] A. Sørensen and K. Mølmer, ‘Quantum computation with ions in thermal motion’, *Phys. Rev. Lett.* **82**(9), 1971–1974 (1999). [doi:10.1103/PhysRevLett.82.1971](https://doi.org/10.1103/PhysRevLett.82.1971)
- [24] D. Jonathan and M. B. Plenio, ‘Light-shift-induced quantum gates for ions in thermal motion’, *Phys. Rev. Lett.* **87**(12), 127901 (2001). [doi:10.1103/PhysRevLett.87.127901](https://doi.org/10.1103/PhysRevLett.87.127901)
- [25] D. F. V. James, ‘Quantum computation with hot and cold ions: an assessment of proposed schemes’, *Fortschritte der Physik* **48**(9–11), 823–837 (2000). [doi:10.1002/1521-3978\(200009\)48:9/11<823::AID-PROP823>3.0.CO;2-M](https://doi.org/10.1002/1521-3978(200009)48:9/11<823::AID-PROP823>3.0.CO;2-M)
- [26] S. E. Hamann, D. L. Haycock, G. Klose, P. H. Pax, I. H. Deutsch, and P. S. Jessen, ‘Resolved-sideband Raman cooling to the ground state of an optical lattice’, *Phys. Rev. Lett.* **80**(19), 4149–4152 (1998). [doi:10.1103/PhysRevLett.80.4149](https://doi.org/10.1103/PhysRevLett.80.4149)
- [27] J.-S. Chen, K. Wright, N. C. Pisenti, D. Murphy, K. M. Beck, K. Landsman, J. M. Amini, and Y. Nam, ‘Efficient-sideband-cooling protocol for long trapped-ion chains’, *Phys. Rev. A* **102**(4), 043110 (2020). [doi:10.1103/PhysRevA.102.043110](https://doi.org/10.1103/PhysRevA.102.043110)
- [28] R. J. Hendricks, J. L. Sørensen, C. Champenois, M. Knoop, and M. Drewsen, ‘Doppler cooling of calcium ions using a dipole-forbidden transition’, *Phys. Rev. A* **77**(2), 021401(R) (2008). [doi:10.1103/PhysRevA.77.021401](https://doi.org/10.1103/PhysRevA.77.021401)
- [29] J. J. García-Ripoll, P. Zoller, and J. I. Cirac, ‘Speed optimized two-qubit gates with laser coherent control techniques for ion trap quantum computing’, *Phys. Rev. Lett.* **91**(15), 157901 (2003). [doi:10.1103/PhysRevLett.91.157901](https://doi.org/10.1103/PhysRevLett.91.157901)